Available online at www.sciencedirect.com
SCIENCE DIRECT®
Journal of Power Sources 136 (2004) 66–71
JOURNAL OF POWER SOURCES
www.elsevier.com/locate/jpowsour

Fabrication and properties of anode-supported tubular solid oxide fuel cells

Yanhai Du*, N.M. Sammes

Connecticut Global Fuel Cell Center, University of Connecticut, 44 Weaver Rd, Storrs 06269-5233, USA

Received 28 April 2004; accepted 20 May 2004

Available online 27 July 2004

Abstract

Tubular solid oxide fuel cell (SOFC) systems have many desirable characteristics over their planar counter-parts. Anode-supported tubes provide an excellent platform for individual cells. They allow for a thin electrolyte layer to be applied to the outside of the tube, which helps to minimize polarization losses. This paper describes the fabrication of nickel–zirconia (Ni–YSZ)-based anode tubes via extrusion of a plastic mass through a die of the required dimensions. The anode tubes were then dried and fired. Tests were performed on the tubes to determine the effects of firing temperature on porosity to allow for a pinhole-free electrolyte coating to be applied. Thin layer coating techniques, including vacuum-assisted dip coating and painting, were compared. Ni–YSZ anode-supported tubular SOFCs with a gas-tight thin YSZ electrolyte layer were then realized. Microstructure of the anode support, electrolyte and cathode thin films was also examined.
© 2004 Published by Elsevier B.V.

Keywords: Fabrication; Property; Design; Solid oxide fuel cell

1. Introduction

Solid oxide fuel cells (SOFCs) are promising candidates for many power generation schemes from small systems of a few watts up to megawatt-sized power plants. They have a high thermodynamic efficiency and can operate on many different fuels [1]. The two major stack designs can be classified as planar and tubular. Tubular systems have advantages, including higher mechanical and thermal stability [2] and simpler seal requirements. Planar systems, however, require gas sealing between each cell and around all edges and manifolds, each of which is at the cell's operating temperature. Tubular stacks only require sealing where the manifolds connect to the cells; this area can be kept outside of the active cell zone where temperatures will be lower. Using an anode support allows a thin-coated electrolyte to be placed on the supporting anode, which reduces electrolytic resistance losses and yields better conductance at lower temperatures over an electrolyte support. Fabrication is one of the major focuses of cost reduction. Although tubular SOFC technology has been well published [3–6], there is limited information on the fabrication processes [7–9] and lack of knowledge about extrusion of anode-supported tubular SOFCs [10–12]. The purpose of this study was to optimize fabrication processes for these tubular cells and gain knowledge of the relationship between the processing and the properties. The cell configuration used in this project was a nickel and yttria-stabilized zirconia (Ni–YSZ) cermet anode-supported tube with a thin YSZ electrolyte coat and a thin lanthanum strontium magnate (LSM) cathode.

2. Experimental

NiO–YSZ tubes were extruded from a plastic mass through a die forming a 17 mm outside diameter. The mass was created by mixing commercially available nickel oxide–YSZ powder (equivalent to 50% nickel and 50% YSZ by volume) (Fuel Cell Materials), and polymer binders, polyvinyl alcohol (PVA) and methylcellulose (The Dow Chemical Company). This was mixed with water for 1–2 h and left to age overnight. A vacuum was applied to the mixing chamber for 10–30 min to remove air from the mass. The mass was extruded using a ram extruder, with an in-house designed die. After drying, the tubes were cut to length and then pre-fired to various temperatures in air for the electrolyte coating step. The nickel oxide was reduced to nickel for electrical conduction as described below.

* Corresponding author. Tel.: +1 860 486 5686; fax: +1 860 486 8378.
E-mail address: ydu@engr.uconn.edu (Y. Du).

0378-7753/$ – see front matter © 2004 Published by Elsevier B.V.
doi:10.1016/j.jpowsour.2004.05.028

The pre-fired anode tubes were dip-coated in a YSZ slurry (Fuel Cell Materials) with vacuum assistance. The pre-fire temperature, submersion time and vacuum pressure were varied to determine the best conditions for a dense coating. The coatings were left to dry in air, then placed in an oven at approximately 50 °C before sintering at 1450–1500 °C.

Even though the coatings may appear crack-free, they must still be checked for gas tightness. The anode becomes dense after the coating is fully sintered. To test the coating for gas tightness, the anode must be reduced. A quartz reduction chamber was used to contain a reducing atmosphere while being heated to 800 °C. Nitrogen was used to purge up to 200 °C, then hydrogen was passed through the chamber at approximately 0.5 L/min until the temperature returned to 200 °C on cool down, when nitrogen was again purged until room temperature was reached. The reduced porous tubes allowed for testing of the electrolyte coating. Two methods were used to test the thin electrolyte for gas tightness. A vacuum was applied to the inside of the tube and the vacuum decay over time was measured and used to evaluate the gas tightness. The tube was also pressurized using nitrogen and submerged in water; bubbles would form if cracks, pinholes or through-pores were present in the electrolyte. The cathode layer was applied using a brush painting method and $La_{0.8}Sr_{0.2}MnO_3$ (LSM) ink (American Elements), followed by firing to 1100 °C in air.

The apparent density of the porous anode samples was measured using a helium gas absorption pycnometer (Micromeritics). The porosity was calculated according to the apparent density and bulk density. Pore size and pore size distribution were obtained using a mercury intrusion porosimetry and capillary flow porometry (Porous Materials, Inc.). The modulus of rupture (MOR) was determined using an Instron material tester and a three-point bending test fixture on the extruded and fired tubes. Light microscopy and scanning electron microscope (SEM) were used to examine the microstructure of the coating.

Table 1
Pore size and pore size distribution of anode tubes measured by mercury porosimetry

Pore diameter (μm)	Pore volume (%)
<40	79
<15	17
<4.5	2.5
<0.06	1.5

3. Results and discussion

3.1. The tubes

After drying, the extruded anode support tubes were round and straight. The final tube dimensions of the fired tubes (diameter, wall thickness and length) can be determined according to the cell/stack design, extrusion die and the control of the process parameters, for example, the firing temperature. During firing, the tubes had a minimal shrinkage change up to about 1000 °C; however, above this temperature, the shrinkage increased rapidly with respect to temperature. Fig. 1 is a plot of tube firing shrinkage as a function of sintering temperature. This figure also shows the tube strength (MOR) corresponding to the firing temperature. The tubes were very weak in the temperature range of 200–1000 °C because the green tubes lost binding strength after the binder was burned out and the ceramic bonding had

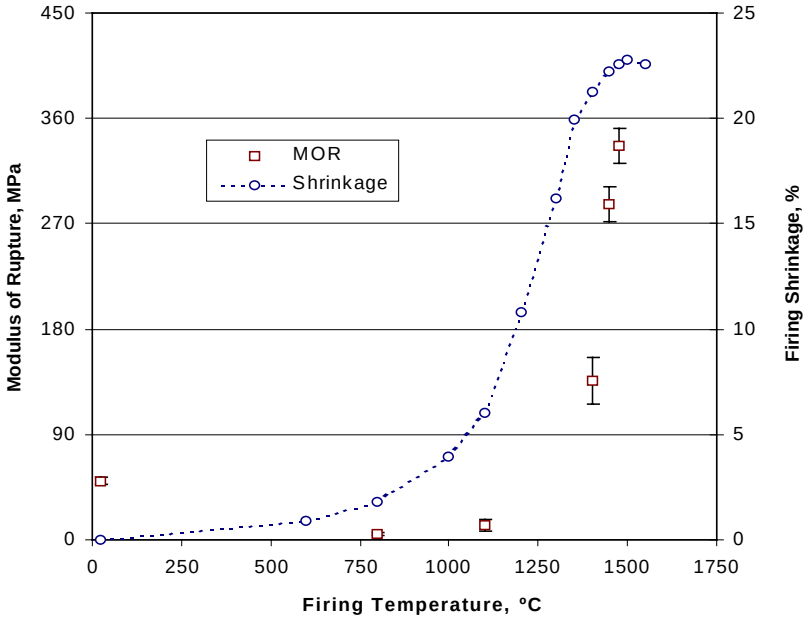

Fig. 1. Effect of firing temperatures on MOR and shrinkage of anode tubes.

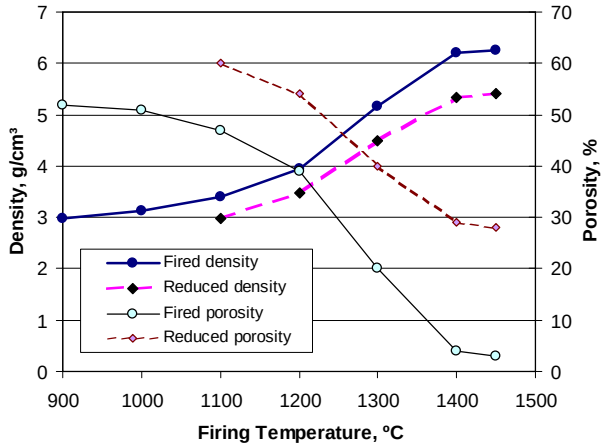

Fig. 2. Effect of firing temperature on anode density and porosity.

not formed. The fired body shrank over 15% between 1100 and 1400 °C, indicating that the material had been sintered. The shrinkage was accompanied by a significant increase in the MOR. Fig. 2 shows the correlation between the firing temperature and the density/porosity of the anode tubes. The materials increased in density as the firing temperature approached 1400 °C, while the porosity significantly decreased to below 5%. The porosity, however, recovered approximately 20–25% on reducing the anode (NiO to Ni). The reduction of the anode (65 wt.% NiO and 35 wt.% YSZ, equivalent to 50 vol.% Ni and 50 vol.% YSZ) resulted in a 13.9% mass reduction. The dimensional changes of the anode during reduction were negligible. This was postulated as being due to the stable zirconia network supporting the structure. Theoretically, in this NiO–YSZ cermet with a YSZ stable skeleton, reducing NiO to Ni will cause 25% porosity (density: NiO 6.70 g/cm^3, Ni 8.90 g/cm^3).

The pore size distribution (Fig. 3) measured by mercury porosimetry suggested that most of the pores were in the micrometer range, and 96 vol.% of the pores were in the range of 4.5–40 μm (Table 1) [13]. SOFCs consist of a porous anode, a porous cathode and a dense electrolyte. The electrode porosity and pore structure affect the cell performance. Using a capillary flow porometry technique, it was revealed that the largest through-pore diameter was 0.152 μm and the mean flow pore diameter was 0.052 μm. These results suggest that the materials contained many blind pores that are less useful than the through-pores for gas diffusion in SOFCs. The anode tube final firing temperature should balance both the mechanical and porosity requirements.

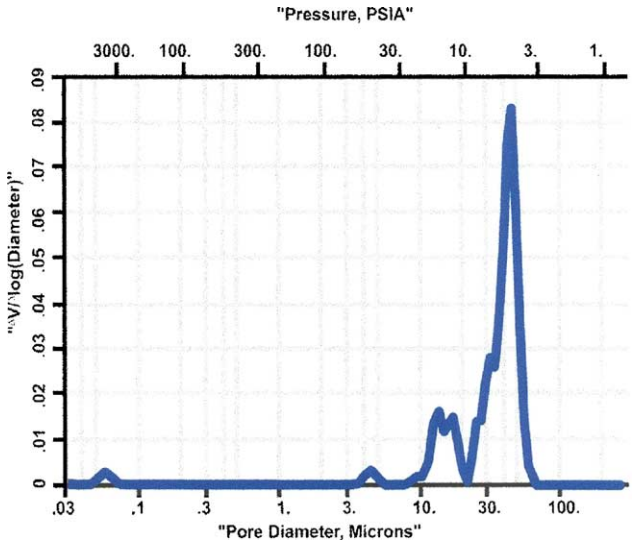

Fig. 3. Pore size distribution of anode tubes fired at 1450 °C [13].

3.2. Electrolyte and cathode coating

The electrolyte is one of the key that significantly affects the final performance of the product. The electrolyte must be dense enough to avoid gas leakage and thin enough to reduce the ohmic resistance. The vacuum-assisted slurry coating gave a uniform electrolyte layer. However, the major objective to achieve a gas-tight thin layer was to obtain pinhole-free and microcrack-free coatings at the green stage. If the coating is applied too thick, it cracks. Multiple dips were attempted to even out the layers and build overall thickness without cracking. However, since the first coating filled most of the pores, the vacuum for the subsequent coats was no longer as effective as for the first coat.

A crack formation time line was made to determine when cracks were formed. Fig. 4 shows pictures of the same tube during various points on this time line. There was no crack observed on the coating surface after drying in air for less than 1 h (see Fig. 4a). The crack formation started at the latter stages of the drying step (Fig. 4b), and the cracks further developed during the rest of the drying (Fig. 4c) and finally became more defined after sintering (Fig. 4d). It was found that there was no crack development during the firing stage on samples that had no cracks after drying. This observation suggested that the cracks were formed during the middle-to-late stages of drying and grew throughout the drying process.

Using a thin slurry, applying a thin coat and drying slowly were helpful in reducing the formation of cracks. Dip coating was tried on fully fired tubes, but runs and drips formed, causing extensive cracking. There was a large variation of coating thickness of the brush-painted electrolyte layer due to the bristles of the brush.

The effects of the major coating parameters (pre-fire temperatures, submersion time, and vacuum pressure and number of coats) on coating quality were examined using the same YSZ slurry, and the results are summarized in Table 2. The measures used to describe the coating quality (defects) under optical microscopy (magnification 1000 times) were the appearance of microcracks, cracks, pinholes, pockmarks and nonwetted spots as illustrated in Fig. 5. The presence of nonwetted spots, pinholes and cracks would cause leakage, while pockmarks did not result in leakage because they were covered by electrolyte coatings. Table 2 postulates that:

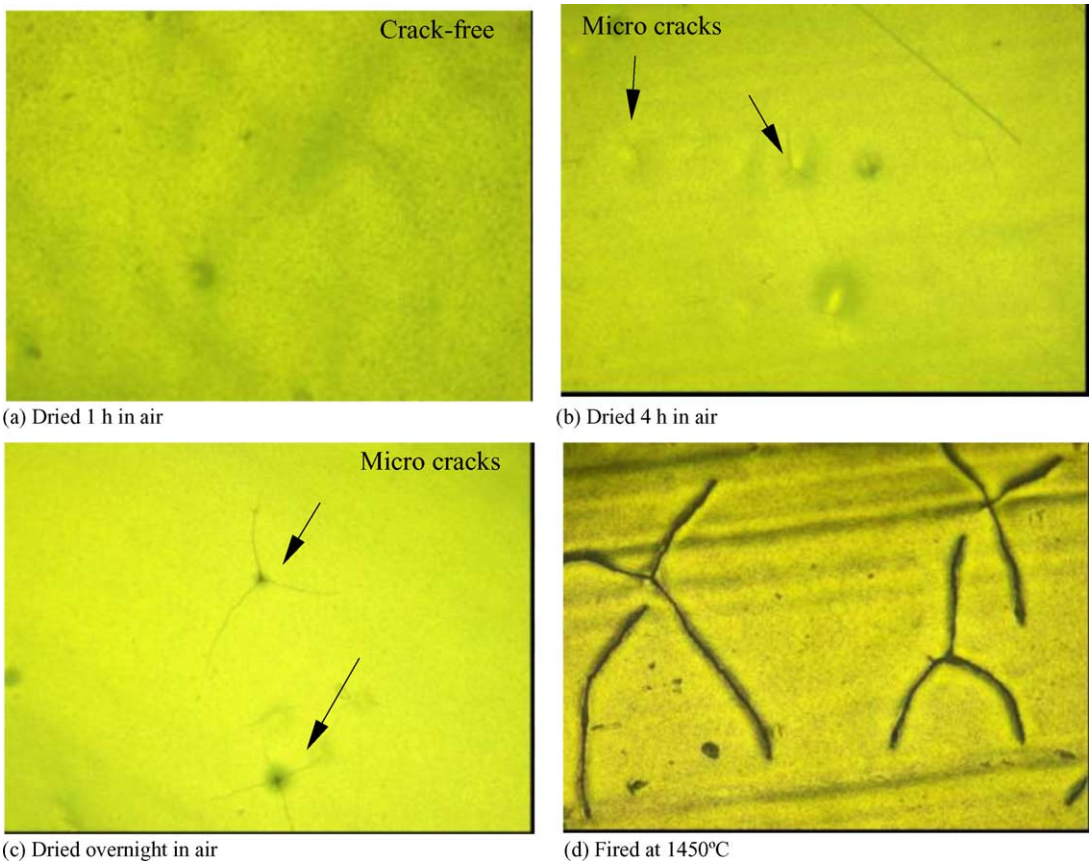

Fig. 4. Light optical photos of the YSZ electrolyte surfaces (a–c) during drying and (d) after sintering.

Table 2
Effects of the pre-firing temperature, vacuum pressure, submersion time and number of coats on the coating quality

Pre-firing temperature (°C)	Vacuum pressure (in. Hg)	Submersion time for each coat (s)	Number of coats	Optical observations on YSZ coatings sintered at 1450 °C for 2 h
1100	25	10	1	Microcracks
			2	Cracks
			3	Large cracks, peels off
1100	0	10	1	Microcracks
	5			Very few microcracks
	10			Few microcracks, pockmarks
	20			Microcracks
900	10	10	1	Microcracks, pockmarks
1000				No microcracks, pockmarks
1200				Short cracks, nonwetted spots
1300				Cracks, nonwetted spots

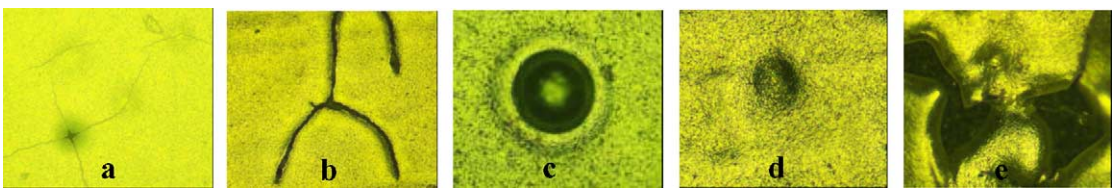

Fig. 5. Measures of electrolyte coating defects: (a) microcracks, (b) cracks, (c) pockmarks and (d) nonwetted sports.

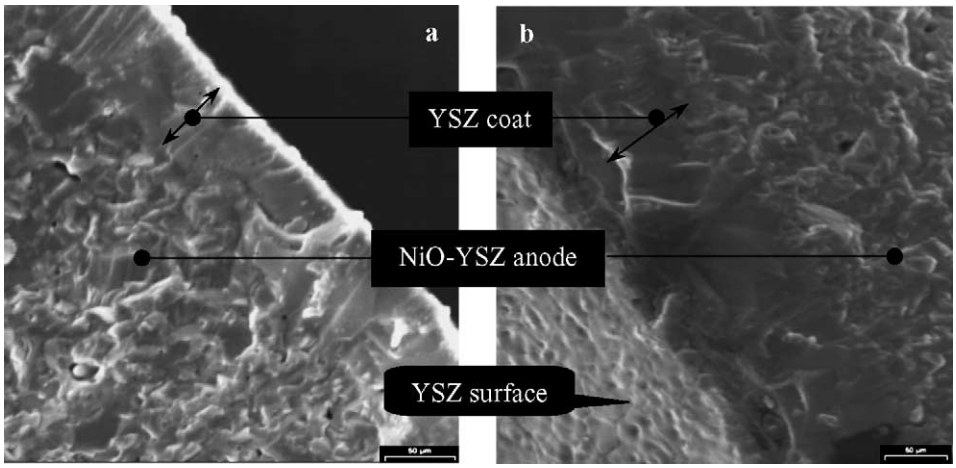

Fig. 6. SEM images of fracture surface of the YSZ coated anodes after sintering at 1450 °C for 2 h. The anodes were pre-fired at (a) 1100 °C and (b) 1000 °C.

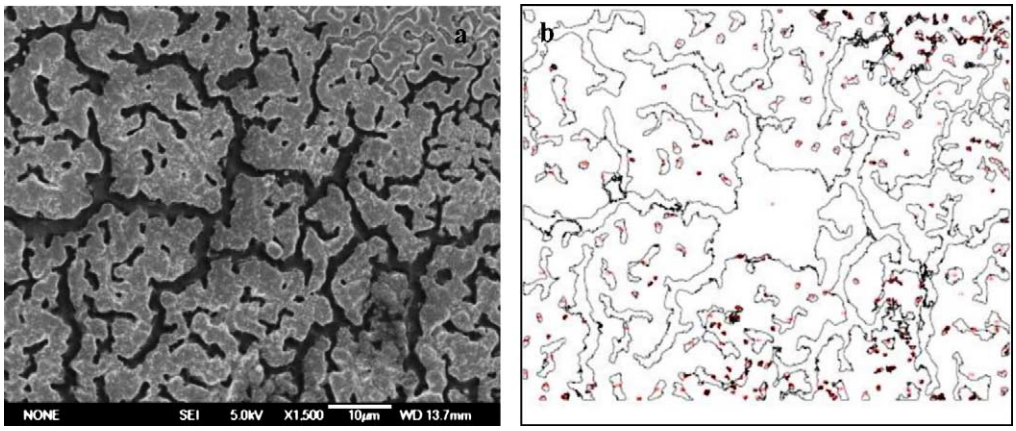

Fig. 7. (a) SEM micrograph of sintered cathode and (b) the image object process result [14].

1. At high vacuum (25 in. Hg), as more coats are applied, cracking becomes more severe. One coat for 10-s submersion time was better than multiple coats, and also longer submersion times (>10 s) resulted in a thicker coating and more cracks after drying and sintering.
2. Varying the vacuum between 0 and 20 in. Hg, while keeping the submersion time at 10 s and one coat, indicated that vacuum at 5–10 in. Hg gave a better coating. Dipping without a vacuum did not produce a uniform coating, and runs and drips formed causing thick areas, which cracked during drying.
3. The effect of pre-firing temperature was clear: the tubes pre-fired at temperatures lower than 1000 °C had higher porosity (50%, see Fig. 2) and larger pore size, which resulted in a thicker coat; on the other hand, the tubes fired at higher temperatures caused nonwetted spots, due to the sintered surface, had low wettability to the slurry.

Overall, the optimized coating conditions were: one coat on 1000–1100 °C pre-fired tubes at 5–10 in. Hg vacuum for 5–10 s. The tubes coated in these conditions had a sintered electrolyte thickness of 10–50 μm depending on the viscosity of the slurry.

SEM micrographs of the sintered electrolyte coat (Fig. 6) indicated that the YSZ electrolyte layer was dense and well bound with the anode. Leakage tests were conducted on the reduced anode with electrolyte and the electrolyte was observed to be gas tight.

Thin cathode coatings were applied on top of the sintered electrolyte and then fired to adhere. Mud-crazes were observed on the surface of the sintered cathode under the SEM (Fig. 7). Analyzing the image, using image software (Image-J), showed a 25% porosity of the cathode [14]. Future work will examine the electrical properties of the single cell and a small stack, and will be the subject of a future publication.

4. Conclusion

Anode-supported tubes and single fuel cells were prepared by plastic extrusion, and vacuum-assisted dip coating

and painting techniques. The mechanical strength of sintered (1450–1500 °C) anode tubes was approximately 300 MPa. The pre-fired (1000–1100 °C) anode support provided an excellent platform for thin film application. Challenges to achieve microcrack-free thin electrolyte layers were addressed. The microcracks were found to start at the latter stages of drying. Gas-tight thin YSZ layers (10–50 μm) were obtained after sintering. The sintered electrolyte layer bound well with the porous anode. The porosities of the cathode and reduced anode were 25–30%.

References

[1] S.C. Singhal, K. Kendal (Eds.), High Temperature Solid Oxide Fuel Cells: Fundamental, Design and Applications, Elsevier, 2003, pp. 15–55.
[2] Y. Du, N.M. Sammes, G.A. Tompsett, D. Zhang, J. Swan, M. Bowden, J. Electrochem. Soc. 150 (1) (2003) A74.
[3] K. Kendall, M. Prica, in: U. Bossel (Ed.), Proceedings of the First European Solid Oxide Fuel Cell Forum, Lucerne, Switzerland, 1994, p. 163.
[4] R.J. Bratton, P. Singh, in: P.N. Kumta, G.S. Rohrer, U. Balachandran (Eds.), Ceramic Transactions, The American Ceramic Society, Weterville, Ohio, 1995, pp. 239–262.
[5] R.A. George, N.F. Bessette, J. Power Sources 71 (1998) 131.
[6] S.C. Singhal, in: Proceedings of the 12th International Conference on Solid State Ionics, Greece, 1999.
[7] B.P. Borglum, US patent 6,217,822 B1, United States Patent and Trademark Office, 2001.
[8] R.N. Basu, C.A. Randall, M.J. Mayo, in: S.C. Singhal (Ed.), Proceedings of the Fuel Cell Seminar, 2001, p. 266.
[9] Y. Du, Fabrication and characterization of micro-tubular solid oxide fuel cells, Ph.D. dissertation, The University of Waikato, Hamilton, 2004, p. 200.
[10] I.P. Kilbride, J. Power Sources 61 (1996) 167.
[11] H. Negishi, N. Sakai, K. Yamaji, T. Horita, H. Yokokawa, in: S.C. Singhal, M. Dokiya (Eds.), Proceedings of the Solid Oxide Fuel Cells (SOFC VI), The Electrochemical Society, Inc., Hawaii, 1999, pp. 885–892.
[12] R.H. Song, K.S. Song, Y.E. Ihm, H. Yokokawa, in: H. Yokokawa, S.C. Singhal (Eds.), Proceedings of the Seventh International Symposium on Solid Oxide Fuel Cells (SOFC VII), The Electrochemical Society, Inc., Tsukuba, Japan, 2001, p. 1073.
[13] K. Gupta, Y. Du, A. Jena, N.M. Sammes, Presented at First International Conference on Fuel Cell Development and Deployment, Storrs, Connecticut, 2004.
[14] N.M. Sammes, Y. Du, N. Padture, M. Wei, X. Huang, G. Ju, J. Wu, K. Reifsnider, Presented at First International Conference on Fuel Cell Development and Deployment, Storrs, Connecticut, 2004.